ISSN 0006-2979, Biochemistry (Moscow), 2024, Vol. 89, No. 7, pp. 1260-1272 © The Author(s) 2024. This article is an open access publication.

Structural Basis for Evasion of New SARS-CoV-2 Variants from the Potent Virus-Neutralizing Nanobody Targeting the S-Protein Receptor-Binding Domain

Nikolai N. Sluchanko[1,2,a]*, Dmitry V. Shcheblyakov[2,b]*, Larisa A. Varfolomeeva[1], Irina A. Favorskaya[2], Inna V. Dolzhikova[2], Anastasia I. Korobkova[2], Irina A. Alekseeva[2], Ilias B. Esmagambetov[2], Artem A. Derkaev[2], Vladimir V. Prokofiev[2], Ilya D. Zorkov[2], Denis Y. Logunov[2], Alexander L. Gintsburg[2], Vladimir O. Popov[1], and Konstantin M. Boyko[1,2,c]*

[1]*Bach Institute of Biochemistry, Federal Research Centre "Fundamentals of Biotechnology", Russian Academy of Sciences, 119071 Moscow, Russia*

[2]*National Research Center for Epidemiology and Microbiology named after Honorary Academician N. F. Gamaleya, Ministry of Health of the Russian Federation, 123098 Moscow, Russia*

[a]*e-mail: nikolai.sluchanko@mail.ru* [b]*e-mail: sdmitriyv@mail.ru* [c]*e-mail: kmb@inbi.ras.ru*

Received May 16, 2024
Revised June 4, 2024
Accepted June 6, 2024

Abstract—COVID-19 has caused millions of deaths and many times more infections worldwide, emphasizing the unpreparedness of the global health system in the face of new infections and the key role for vaccines and therapeutics, including virus-neutralizing antibodies, in prevention and containment of the disease. Continuous evolution of the SARS-CoV-2 coronavirus has been causing its new variants to evade the action of the immune system, which highlighted the importance of detailed knowledge of the epitopes of already selected potent virus-neutralizing antibodies. A single-chain antibody ("nanobody") targeting the SARS-CoV-2 receptor-binding domain (RBD), clone P2C5, had exhibited robust virus-neutralizing activity against all SARS-CoV-2 variants and, being a major component of the anti-COVID-19 formulation "GamCoviMab", had successfully passed Phase I of clinical trials. However, after the emergence of the Delta and XBB variants, a decrease in the neutralizing activity of this nanobody was observed. Here we report on the successful crystal structure determination of the RBD:P2C5 complex at 3.1 Å, which revealed the intricate protein–protein interface, sterically occluding full ACE2 receptor binding by the P2C5-neutralized RBD. Moreover, the structure revealed the developed RBD:P2C5 interface centered around residues Leu452 and Phe490, thereby explaining the evasion of the Delta or Omicron XBB, but not Omicron B.1.1.529 variant, as a result of the single L452R or F490S mutations, respectively, from the action of P2C5. The structure obtained is expected to foster nanobody engineering in order to rescue neutralization activity and will facilitate epitope mapping for other neutralizing nanobodies by competition assays.

DOI: 10.1134/S0006297924070083

Keywords: crystal structure, protein–protein interaction, neutralizing antibodies

INTRODUCTION

Infectious disease outbreaks, whether pandemic or seasonal, impose significant economic and social burdens. The therapeutic use of virus-neutralizing antibodies has emerged as a promising strategy against certain infectious diseases [1-5]. However, the continual evolution of viral strains during ongoing epidemics can undermine the effectiveness of existing treatments. Mutations in emerging variants can diminish the potency of established antibody therapies [6], underscoring the need for detailed structural insights into virus-neutralizing antibody epitopes to bolster therapeutic design through protein engineering methods [7, 8].

* To whom correspondence should be addressed.

Amidst the COVID-19 (Coronavirus disease 2019) pandemic, which has claimed over 7 million lives globally from 2019 to April 2024 (https://covid19.who.int), researchers worldwide have mobilized efforts to develop monoclonal antibodies with potent virus-neutralizing capabilities. These efforts have predominantly targeted the SARS-CoV-2 (severe acute respiratory syndrome-related coronavirus 2) surface glycoprotein (S, or Spike protein), aiming to disrupt its interaction with the ACE-2 cellular receptor and thwart viral entry into human cells [9-13].

In the National Research Center for Epidemiology and Microbiology, named after Honorary Academician N. F. Gamaleya of the Ministry of Health of the Russian Federation, a drug called GamCoviMab based on a mix of two neutralizing antibodies, including the P2C5 clone, has been developed (https://classic.clinicaltrials.gov/ct2/show/NCT05729360). This drug demonstrated efficacy in a model of lethal ACE-2 transgenic mouse infection with various SARS-CoV-2 variants, including the Omicron BA.1, BA.2, and BA.5 variants. Evaluation of the drug's *in vitro* virus-neutralizing activity against these Omicron variants revealed a minimum effective concentration of less than 1.2 μg/ml [14, 15]. P2C5-containing preparation has successfully passed Phase I of clinical trials. However, after the emergence and wide distribution of the Delta coronavirus variant harboring an L452R mutation and Omicron XBB.1 variant harboring an F490S mutation in the receptor-binding domain (RBD), a decrease in the neutralizing activity of this clone was found.

Novel SARS-CoV-2 variants, such as Delta and Omicron lineages, have raised substantial concerns due to their potential to evade immune responses and resist current therapeutic interventions based on previously very potent neutralizing antibodies [16-19]. In response to these evolving challenges, research into the mechanism of neutralization and antibody evasion by novel variants with mutated RBD of the S protein has garnered significant attention.

This study reports on the successful crystal structure determination and analysis of the complex between the virus-neutralizing single-chain antibody P2C5 and either glycosylated or deglycosylated forms of the Wuhan SARS-CoV-2 S RBD.

MATERIALS AND METHODS

Cell lines and viruses. CHO-S cell line was purchased from Thermo Fisher Scientific (USA), cat. no. R80007. VeroE6 cells (ATCC CRL 1586) were obtained from the Russian Collection of Cell Cultures of Vertebrates (CCCV). Cells were cultured at 37°C and 5% CO_2 in Dulbecco's Modified Eagle Medium (DMEM; Gibco, Switzerland), supplemented with 10% (v/v) fetal bovine serum (Hyclone/Cytiva, USA).

SARS-CoV-2 strains B.1.1.1 (Wuhan D614G, hCoV-19/Russia/ Moscow_PMVL-1/2020), B.1.617.2 (Delta, hCoV-19/Russia/SPE-RII-32758S/2021), B.1.1.529.1 (Omicron BA.1, hCoV-19/Russia/MOW-Moscow_PMVL-O16/2021), Omicron XBB.1.17.2 (hCoV-19/Russia/SPE-RII-4422S/2022) were isolated from nasopharyngeal swabs.

The bacterial strain *Escherichia Coli* Rosetta (DE3) was purchased from Merck-Millipore (USA), cat. no. 70954.

Recombinant proteins expression and purification. Plasmid DNA containing P2C5 coding sequence was transformed into *E. coli* Rosetta DE3 (Merck-Millipore). The transformed cells were cultured in 2xYT medium supplemented with ampicillin (100 μg/ml) at 37°C at 210 rpm to OD_{600} 0.5-0.8. Then IPTG (Anatrace, USA) was added (0.1 mM) and the culture was grown at 30°C overnight. Recombinant P2C5 with a C-terminal 6×His-tag was isolated from the *E. coli* periplasm by cold osmotic shock and purified by metal-ion affinity chromatography, as described in previous work [15, 20]. Also, P2C5 VHH was transformed to a P2C5-Fc format by fusing P2C5 nucleotide sequence to the human IgG1 Fc-fragment sequence. The obtained construction was cloned into the mammalian expression vector pCEP4 (Thermo Fisher Scientific).

The Spike protein receptor-binding domain (RBD) sequences of different variants of SARS-CoV-2 (Wuhan-Hu-1, Gamma, Delta, and Omicron XBB) and also N-terminally truncated RBD of Wuhan-Hu-1 variant sequence (coding amino acid residues 333-541) were cloned into the pCEP4 vector. The information concerning RBD sequences and mutations are summarized in Fig. 4b. The RBD expression constructs contained C-terminal polyhistidine tags for further purification steps.

For recombinant protein expression, CHO-S cells (Thermo Fisher Scientific) were transfected with the obtained pCEP4 vectors using the CHOgro™ Expression System (Mirus Bio, USA) according to the manufacturer's instructions. Polyhistidine-tagged recombinant proteins were purified from cell culture supernatants using metal-ion affinity chromatography resin Sepharose 6 Fast Flow, AKTA Start system and HisTrap HP column (Cytiva). The second purification step was performed using size exclusion chromatography resin Superdex 200 (Cytiva). P2C5-Fc was purified using HiTrap Protein A (Cytiva). The purity of recombinant

Abbreviations: ACE2, angiotensin-converting enzyme 2; CDR, complementarity-determining region; COVID-19, Coronavirus disease 2019; RBD, receptor-binding domain; RMSD, root-mean-square deviation of atomic positions; SARS-CoV-2, severe acute respiratory syndrome-related coronavirus 2.

proteins was assessed by Coomassie Blue staining of SDS-PAGE gels.

Peptide-N-Glycosidase F (PNGase F) for optional RBD deglycosylation was produced in the recombinant form in previous work [20].

ELISA. 96-well immunoplates (Greiner, Austria) were coated with antigens (1 μg/ml) overnight at 4°C. Wells were blocked with 5% non-fat milk (PanReac AppliChem, Spain) in phosphate-buffered saline with 0.05% Tween-20 (TPBS). Serial three-fold dilutions of P2C5 (10 μg/ml to 4.5 ng/ml) were added to the wells. Then horseradish peroxidase (HRP)-conjugated rabbit anti-Myc tag antibodies (ab1326, Abcam, UK) were added. EC50 values were calculated using GraphPad Prism 7 software. In this study, we used the following antigens: receptor-binding domains of spike proteins of Wuhan, Gamma, Delta and XBB.1 virus variants, S1 subdomain of spike protein of Omicron B.1.1.529 variant (Sino Biological) (RBD mutations in this variant are the same as in Omicron BA.1).

Virus neutralization assay. Neutralization assay with live SARS-CoV-2 was performed as previously described [15]. Serial two-fold dilutions of P2C5 antibodies at concentrations ranging from 20 mg/ml to 1.2 ng/ml were mixed with 100 $TCID_{50}$ of SARS-CoV-2 virus (Omicron XBB.1.17.2 or B.1.1.1). The mixture was incubated for 1 h at 37°C and added to a monolayer of Vero E6 cells. After incubation (96-120 h) at 37°C in 5% CO_2, the neutralizing activity of the antibody was assessed visually by the ability to inhibit the cytopathic effect of the virus (CPE). The minimum neutralizing concentration of P2C5 was determined as the minimum antibody concentration at which complete inhibition of the cytopathic effect was observed. All experiments were performed with three replicates.

***In vivo* protection studies in mice.** Hemizygous angiotensin-converting enzyme 2 (ACE2)-transgenic mice (Tg (K18-ACE) 2Prlmn) 10-12 weeks old were used to evaluate the protective capacity of P2C5-Fc antibodies in an *in vivo* model of SARS-CoV-2 infection. Mice were kept in individually ventilated cages (ISOcage P System from Tecniplast) and had free access to food and water. Procedures with animals were conducted in a biosafety level 3 (BSL3) laboratory. All animal experiments were carried out in strict accordance with the recommendations of the Russian Federation (GOST R 53434-2009; Principles of Good Laboratory Practice).

The mice were randomly divided into groups of 5-8 animals each. Infection of animals was performed via intranasal administration of 1×10^5 $TCID_{50}$ of SARS-CoV-2 virus. In the first experiment, two groups of mice (5 animals per group) were intraperitoneally injected with 5 mg/kg of P2C5-Fc 1 and 6 hours after infection by B.1.1.1 virus variant. The control group (n = 5) was treated with PBS. Animals were monitored for survival rate and weight change for 20 days post infection. Mice with 20% body weight loss were humanely euthanized. In the following experiment, to assess the protective capacity of P2C5-Fc antibodies against Delta (B.1.617.2) SARS-CoV-2 variant, a group of mice (n = 5) was administered intraperitoneally with 5 mg/kg of P2C5-Fc 1 h after B.1.617.2 challenge. Control animals were injected with PBS. All procedures in this study were performed as described above.

Inoculation with SARS-CoV-2 of Omicron B.1.1.529 variant was not lethal in hACE2 mice. To evaluate the therapeutic efficacy of P2C5-Fc against Omicron B.1.1.529, mice (n = 8) were injected intraperitoneally with 10 mg/kg of P2C5-Fc 1 h after infection. A control group of 8 animals received PBS. Viral titer ($TCID_{50}$) was measured in lung tissue 4 days after infection. Lung homogenates were prepared using an MPBio homogenizer. Serial ten-fold dilutions of homogenates were titrated in a monolayer of Vero E6 cells to determine the titer of the infectious virus. The cytopathic effect of the virus was assessed visually after 96 h. $TCID_{50}$ was calculated by the Reed and Muench method. Titers below the limit of detection were taken as 1.5 $\log_{10}$ $TCID_{50}$/ml.

Preparation and crystallization of the RBD-P2C5 VHH complex. The detailed procedure of the preparation of the RBD-P2C5 VHH complex was described earlier [20]. Briefly, the purified proteins were pre-mixed at different ratios and analyzed by size-exclusion chromatography on a Superdex 200 Increase 5/150 column (Cytiva) to empirically determine the ratio corresponding to a slight excess of the nanobody. Then, milligram quantities of the proteins were mixed at this chosen volume ratio, incubated, and the heterodimeric complex was separated from the nanobody excess using Superdex 200 Increase 10/300 column (Cytiva). For RBD deglycosylation, the sample loaded on preparative SEC was first treated with PNGase F for 2 h at room temperature and then overnight in the fridge. The complex fractions were pooled and concentrated before crystal screening using Hampton Research crystallization kits (USA) and an Oryx4 crystallization robot (Douglas Instruments, UK). The best crystals of $RBD_{319-541}$/P2C5-VHH and enzymatically deglycosylated $RBD_{333-541}$/P2C5-VHH complexes were obtained at the following conditions: 0.2 M Ammonium sulfate, 0.1 M Bis-Tris pH 6.5, 25% PEG 3350 and 0.15 M DL-Malic acid pH 7.0, 0.1 M Imidazole pH 7.0, 22% v/v Polyethylene glycol monomethyl ether 550, respectively. 20% ethylene glycol was used as a cryoprotectant.

Crystal structure determination. The structure of the N-terminally truncated and PNGase F-treated RBD (residues 333-541) complexed with P2C5 VHH was solved by molecular replacement using MolRep [21] and RBD (PDB ID 7A91) as a search model, which initially resulted in four RBD copies correctly found

and several misplaced copies requiring manual deletion based on the electron density maps revealed. Further molecular replacement using the partial solution composed of four RBD copies allowed to find eight copies of the nanobody modeled by AlphaFold2 [22] based on the amino acid sequence of P2C5 VHH. Of these eight, only one copy of the nanobody was placed close to an RBD and matched the density. This tentative heterodimeric complex was used as a new search model for molecular replacement procedure in MolRep [21], which allowed us to find four copies of the heterodimeric complex between RBD and the nanobody. This partial solution revealed a strong difference density suggesting the correctness of the partial solution and the presence of more protein molecules in the asymmetric unit. To find those, the heterodimer was again used as a search model in MolRep while using the previously found partial solution composed of the four copies of the complex. Finally, this resulted in placing 5 heterodimeric complexes in the asymmetric unit, enabling the refinement of the complete structure, which was done iteratively using Refmac5 [23] and model building in Coot [24]. The refinement involved backbone H-bond restraints, NCS restraints and use of TLS. At final steps of refinement, the use of the ProSMART option in the Refmac5 and reference structures of RBD (PDB ID 7FAT [25]) and nanobody (PDB ID 3STB [26]) helped improve geometry and the R-factors. The refined model of the heterodimeric complex between $RBD_{333-541}$ and P2C5-VHH was used to also solve the similar structure between P2C5-VHH and untruncated $RBD_{319-541}$ not treated with PNGase F for deglycosylation.

RESULTS AND DISCUSSION

A single-domain camelid antibody P2C5 with potent neutralizing activity against a range of SARS-CoV-2 virus variants has previously been identified [15]. The capacity of P2C5-VHH to recognize the S protein of different SARS-CoV-2 variants was evaluated by ELISA (Fig. 1a). We found that P2C5 exhibited strong binding activity toward the S protein of Wuhan, Gamma, and Omicron B.1.1.529 variants. However, binding to the S protein of Delta and XBB.1 decreased, likely due to the mutations affecting the epitope region. Interestingly, fusing P2C5 with Fc resulted in nearly 10 times more efficient RBD recognition (Fig. 1b).

The ability of P2C5 to neutralize live SARS-CoV-2 virus was investigated by microneutralization assay. The virus was mixed with antibodies and then added to Vero E6 cells. The absence of cytopathic effect in the presence of P2C5 was the key evidence of the antibody's neutralization activity. A combination of current data on virus neutralization by the P2C5 antibody with the previously published data [15] is found in Table 1. We observed that P2C5 completely inhibited the cytopathic effect of SARS-CoV-2 Wuhan D614G (B.1.1.1), Gamma (B.1.1.28/P.1), and Omicron B.1.1.529 variants at concentrations of 24-48 nM. The inhibition of the cytopathic effect of SARS-CoV-2 Delta (B.1.617.2) and Omicron XBB.1.17.2 variants was not observed over a wide range of P2C5 concentrations (to 1500 nM). The *in vitro* neutralization activity data are consistent with binding ability data obtained by ELISA.

The protective capacity of P2C5 against SARS-CoV-2 infection *in vivo* was assessed using hACE2

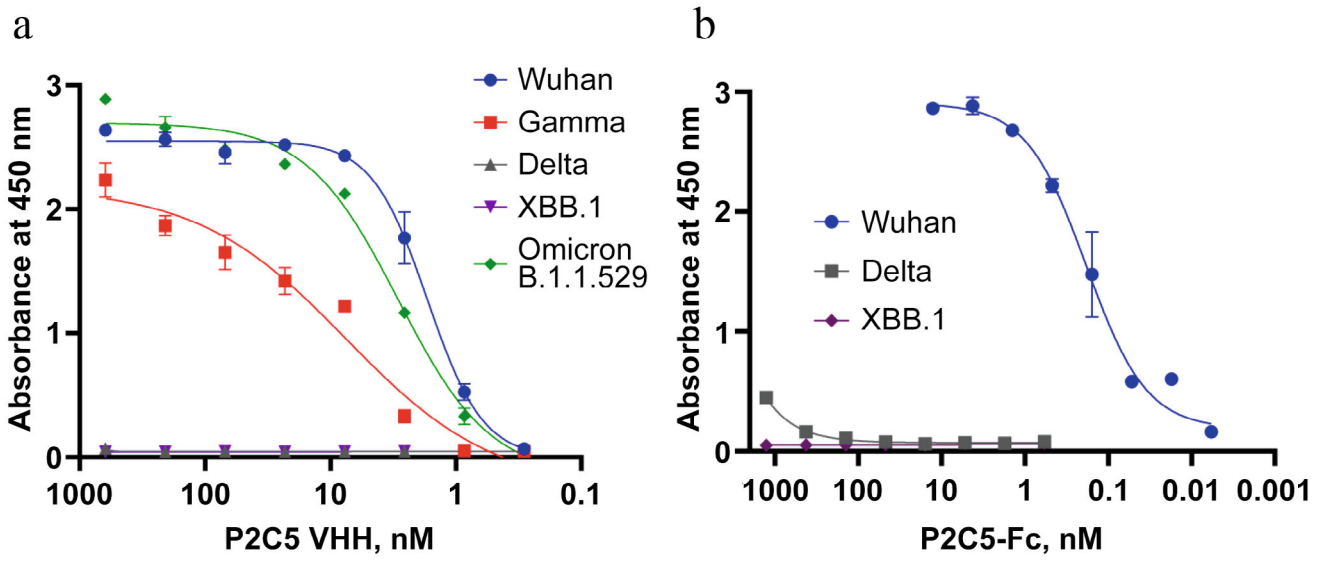

Fig. 1. Recognition of S protein of SARS-CoV-2 variants by P2C5 single-domain antibody (a) or P2C5-Fc (b). The binding of P2C5 to immobilized antigens (RBD of S protein for Wuhan, Gamma, Delta, and Omicron XBB.1 variants and S1 subdomain of S protein for Omicron B.1.1.529 variant) was detected by ELISA. P2C5 bound S protein of Wuhan, Gamma, and Omicron B.1.1.529 variants with half-maximal concentration (EC50) 1.7, 7.6, 2.9 nM, respectively.

Table 1. Neutralizing activity of P2C5 antibody against live SARS-CoV-2 variants

	SARS-CoV-2 virus variant				
	B.1.1.1	Gamma (B.1.1.28/P.1)*	Delta (B.1.617.2)*	Omicron B.1.1.529*	Omicron XBB.1.17.2
Minimum inhibitory concentration of P2C5 VHH, nM	24.04	48.08	>1500	24.04	>1500

* Previously published data from [15].

transgenic mice. For these studies, P2C5 was fused to the human IgG1 Fc-fragment for half-life prolongation. The P2C5-Fc protein was produced in CHO-S cells and purified. We assessed P2C5-Fc therapeutic efficacy against infection caused by three different SARS-CoV-2 variants: Wuhan D614G (B.1.1.1), Delta, and Omicron B.1.1.529.

First, we evaluated the protective effect of P2C5-Fc after B.1.1.1 (Wuhan D614G) and B.1.617.2 (Delta) lethal challenge. Mice were infected intranasally with 1×10^5 $TCID_{50}$ of SARS-CoV-2 and 1 h or 6 h later received 5 mg/kg P2C5-Fc antibodies intraperitoneally. As shown in Fig. 2a, all mice treated with P2C5-Fc survived after B.1.1.1 infection ($p = 0.0004$, log-rank test), furthermore, no weight loss was observed. After infection with the Delta variant of the virus, surprisingly, 40% of antibody-treated animals survived (data not significant, $p = 0.33$, log-rank test), despite the fact that single-domain P2C5 antibody did not recognize the S protein of this variant in ELISA (Fig. 2b). A probable explanation for the revealed potential protection is the capacity of the dimeric Fc-fused form of P2C5 to weakly bind the S protein of Delta (Fig. 1b).

The SARS-CoV-2 Omicron B.1.1.529 variant contains a large number of mutations resulting in non-lethal virulence in hACE2 mice. As all control group mice (treated with PBS after infection) survived and showed no marked weight loss, we assessed the virus load in the lungs of the animals on day 4 after infection (Fig. 2c). Administration of P2C5-Fc 1 h after challenge resulted in a significant reduction of SARS-CoV-2 titer in the lungs ($p = 0.007$, Mann–Whitney test), and the virus content in the antibody-treated group was below the limit of detection (<1.5 $\log_{10}$ $TCID_{50}$/ml). This result highlights the efficacy of P2C5-Fc treatment *in vivo* also against the Omicron B.1.1.529 variant of the SARS-CoV-2 virus.

The differential activity of P2C5 on SARS-CoV-2 variants clearly required mechanistic explanation. To this end, we aimed at crystal structure determination of the RBD:P2C5 complex and subjected the purified complex to extensive crystallization screening [20]. Although this complex readily crystallized under various conditions, it proved difficult to find diffracting crystals and therefore we attempted different sample modifications. In particular, we subjected to crystallization untreated RBD or RBD deglycosylated by recombinant PNGase F [20], in the hope that deglycosylation would reduce the heterogeneity associated with RBD. In addition, RBD was truncated from the N-terminus until residue 333 so that several upstream glycosylated residues were omitted. Wide screening of many crystals using synchrotron X-ray radiation was crucial to finding diffracting crystals for both unmodified $RBD_{319\text{-}541}$:P2C5 and enzymatically deglycosylated $RBD_{333\text{-}541}$:P2C5 complexes (Table 2). Given that the diffraction quality of the two crystals was comparable (3.1 or 3.7 Å), we could finally suggest that deglycosylation on its own was dispensable for obtaining crystals of sufficient quality, which disproved our initial considerations.

The crystal structure was first solved for the minimally glycosylated $RBD_{333\text{-}541}$:P2C5 complex, and the solution was then used to also determine the structure of the $RBD_{319\text{-}541}$:P2C5 complex, which turned to be nearly identical in terms of the relative positions of RBD and P2C5 within the heterodimer [Cα RMSD (root-mean-square deviation of atomic positions) did not exceed 0.5 Å]. Therefore, for further analysis we chose the $RBD_{319\text{-}541}$:P2C5 structure as having the higher resolution (Fig. 3a), which was sufficient to confidently trace most of the core RBD and P2C5 residues into the electron density maps (Fig. 3b).

The asymmetric unit of the crystal contained five copies of the $RBD_{319\text{-}541}$:P2C5 heterodimer totaling 1575 residues (Fig. 3a), and these copies were nearly identical (Cα RMSD did not exceed 0.5 Å) (Fig. 3c). Interestingly, the final refined crystal structure of the heterodimer was notably different from the closest model of the complex predicted by AlphaFold2 (at the end of April 2024), providing Cα RMSD of only 4.6 Å upon superposition of 311 atoms of the complex. Fig. 3d shows the overlay of these two structures aligned by RBD. It is clear that, while AlphaFold2 rather accurately predicted the RBD structure (Cα RMSD between the crystal structure and the model did not exceed 0.5 Å), the model of its complex with the nanobody was inadequate. Intriguingly, the very recently released AlphaFold3

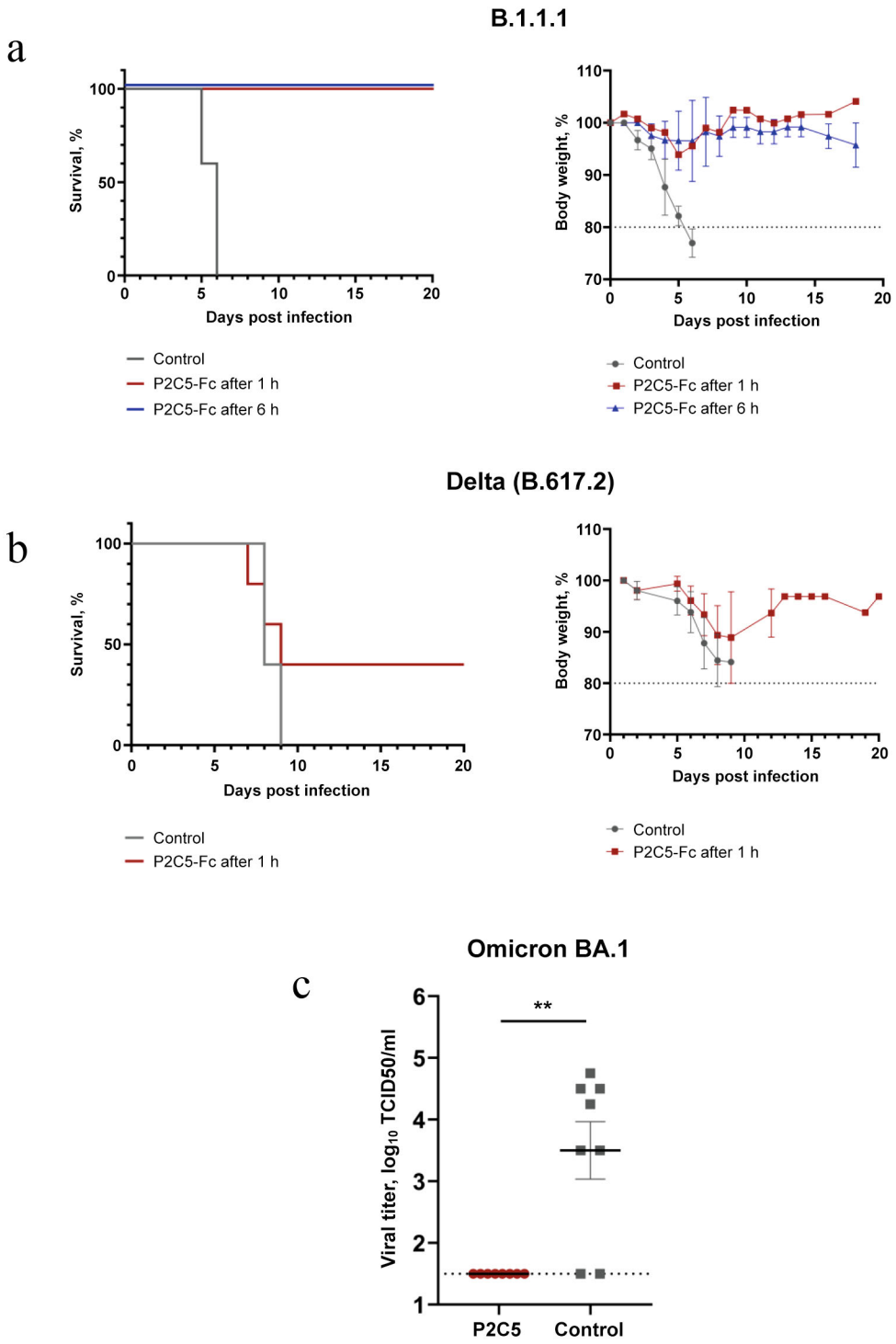

Fig. 2. Therapeutic efficacy of P2C5-Fc against SARS-CoV-2 infection in hACE mice. a-b) Survival rates and mean body weights of mice (n = 5 per group) that were systemically treated (i.p.) with P2C5-Fc 1 h or 6 h after intranasal inoculation of 1×10^5 $TCID_{50}$ of Wuhan D614G (B.1.1.1) or Delta (B.1.617.2) SARS-CoV-2 variants. The control group was treated with PBS 1 h post infection. c) Lung viral titer on day 4 post infection with Omicron B.1.1.529 (1×10^5 $TCID_{50}$ intranasally) in mice injected (i.p.) with 10 mg/kg P2C5-Fc or vehicle (PBS) 1 h after challenge (n = 8 mice per group). Viral titers in the P2C5-Fc group were below the limit of detection of the assay and are shown as 1.5 $\log_{10}$ $TCID_{50}$/ml. ** p = 0.007.

neural network, upgraded for predicting complexes [27], predicted a completely different P2C5 epitope on the opposite side of RBD with respect to the X-ray structure and the AlphaFold2 model (Fig. 3d). These rather poor predictions by superior *in silico* algorithms support the notion that experimental structural biology

Table 2. X-ray data collection and processing

Crystallization condition	$RBD_{333-541}$ complexed with P2C5 nanobody*	$RBD_{319-541}$ complexed with P2C5 nanobody
	0.15 M DL-Malic acid pH 7.0, 0.1 M Imidazole pH 7.0, 22% PEG MME 550	0.2 M $(NH_4)_2SO_4$, 0.1 M Bis-Tris, pH 6.5, 25% PEG 3350
Data collection		
Diffraction source	BL17UM, SSRF	BL17UM, SSRF
Detector	Eiger2 X 16M	Eiger2 X 16M
Wavelength (Å)	0.98	0.98
Temperature (K)	100	100
Space group	$I2_12_12_1$	$P2_12_12_1$
a, *b*, *c* (Å)	126.64, 194.24, 264.37	72.48, 177.46, 209.86
Resolution range (Å)	80.00-3.70 (3.80-3.70)**	48.42-3.10 (3.20-3.10)
Completeness (%)	99.1 (99.6)	98.9 (98.6)
Redundancy	5.0	5.2
$\langle I/\sigma(I)\rangle$	6.6 (0.6)	8.0 (1.5)
R_{meas} (%)	22.8 (316.2)	19.6 (149.5)
$CC_{1/2}$ (%)	99.6 (32.1)	99.3 (45.0)
Refinement		
R_{cryst} (%)	20.7	22.2
R_{free} (%)	26.9	28.3
ML position error, Å	0.57	0.41
No. of non-H atoms		
Protein	12,286	12,255
Other	112	220
Water	0	0
R.m.s. deviations		
Bonds (Å)	0.02	0.02
Angles (°)	3.34	3.01
Ramachandran outliers (%)	3.4	3.7
Average *B* factors (Å^2)		
Protein	195.6	86.4
Other	228.0	145.0
Water	–	–
PDB code	8ZES	8ZER

* Treated with PNGase F for RBD deglycosylation.

** Values for the outer shell are given in parentheses.

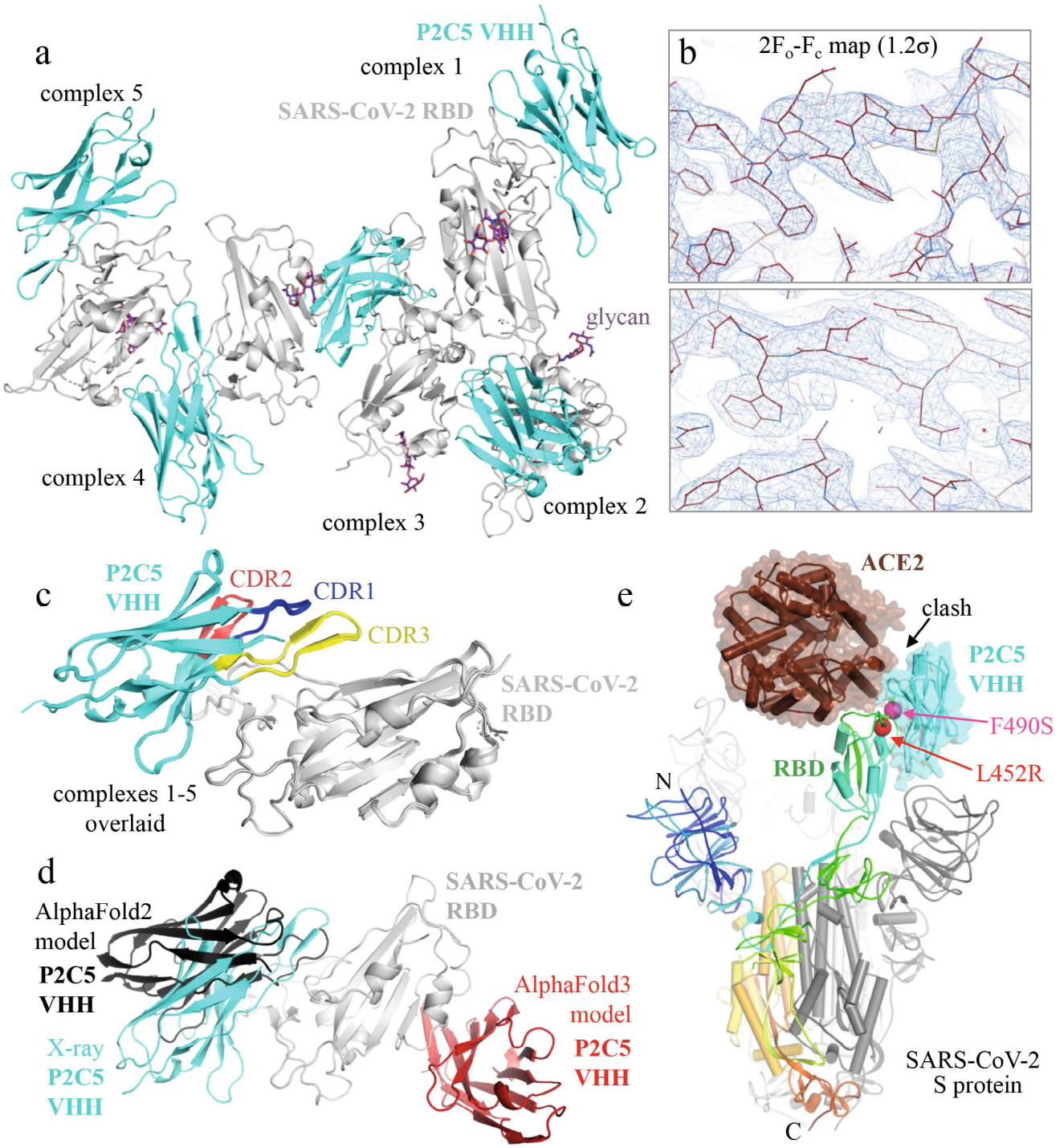

Fig. 3. Structural basis for the virus-neutralizing activity of the P2C5 nanobody. a) Overall view of the asymmetric unit (ASU) of the RBD:P2C5 crystal showing five heterodimers and glycans linked to residue Asn343 of RBD. b) Exemplary fragments of the electron density map contoured at 1.2σ, interpreted with the final refined protein model shown as sticks. c) Structural superposition of the five heterodimer complexes found in the ASU. Complementarity-determining region (CDR) loops 1-3 are highlighted. d) Superposition of the final refined crystal structure of the complex and its best models predicted by AlphaFold2 (black cartoon) or AlphaFold3 (red cartoon) showing inadequacy of the *in silico* models. Cα RMSD of the alignment over the full complex was equal to as large as 4.6 Å for the AlphaFold2 model, whereas AlphaFold3 predicted a completely different P2C5 epitope. e) Overlay of the RBD:P2C5 crystal structure with the ACE2:Spike complex structure determined by cryoelectron microscopy (PDB ID 8WTJ [17]) explaining the neutralization activity of P2C5 nanobody via steric interference with the RBD:ACE2 interaction. One Spike monomer is colored by gradient from N (blue) to C (red) terminus. Red and magenta spheres indicate the location of the L452R and F490S mutations, respectively.

approaches are indispensable for studying antibody complexes in particular.

In the crystallographic heterodimer, the complementarity-determining regions (CDRs) CDR3 (residues 96-110) and CDR2 (residues 50-57) of P2C5 nanobody contributed to the RBD recognition the most, whereas CDR1 (residues 26-33) did not partake in the interaction directly (Fig. 3c). The relative position and orientation of RBD and P2C5 in the crystallographic heterodimer has allowed us to analyze the corresponding

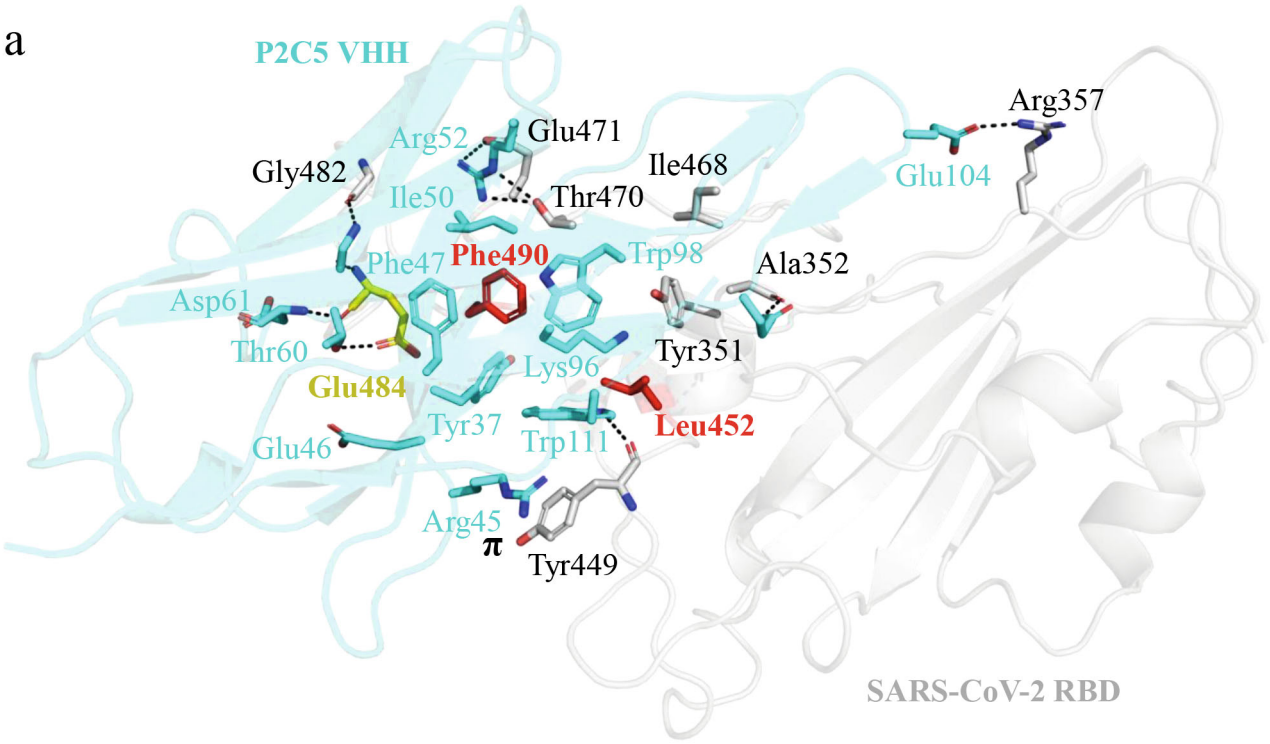

b

SARS-CoV-2	RBD mutations
Wuhan	Genbank accession number MN908947, residues 319-541
Gamma	K417T, **E484K**, N501Y
Delta	**L452R**, T478K
Omicron B.1.1.529	G339D, S371L, S373P, S375F, K417N, N440K, G446S, S477N, T478K, **E484A**, Q493R, G496S, Q498R, N501Y, Y505H
Omicron XBB.1	G339H, R346T, L368I, S371F, S373P, S375F, T376A, D405N, R408S, K417N, N440K, V445P, G446S, N460K, S477N, T478K, **E484A**, F486S, **F490S**, Q498R, N501Y, Y505H

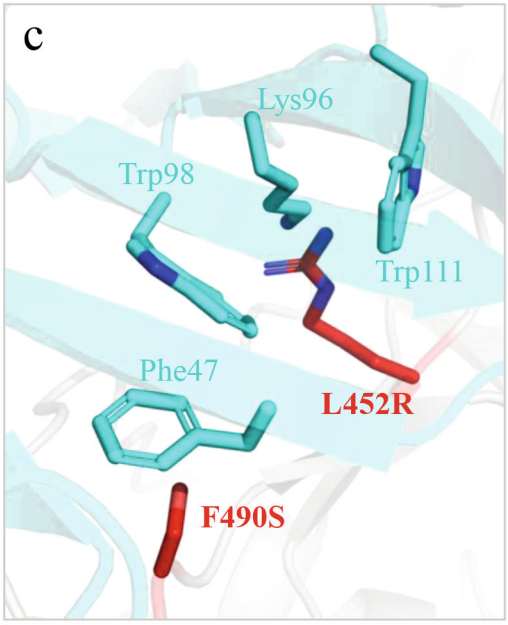

Fig. 4. Structural basis for evasion of the Delta and Omicron XBB.1 variants of SARS-CoV-2 from the action of the neutralizing P2C5 nanobody. a) Crystallographic RBD:P2C5 heterodimer showing the location of key interface contacts. Polar contacts are indicated by dashed lines, key mutated residues are marked by bold font. b) S protein RBD sequence and nonsynonymous mutations in RBD of SARS-CoV-2 variants. Note that RBD of Omicron B.1.1.529 has coinciding mutations as RBD of Omicron BA.1. Key mutations described in the manuscript are highlighted. c) Closeup view of the modeled interface between P2C5 (cyan) and hypothetical RBD containing simultaneous substitutions L452R (Delta) and F490S (Omicron XBB.1).

interface in context of the recently published cryo-EM structure [17] of the XBB Spike protein complexed with the ACE2 receptor (Fig. 3e). This comparison indicated that P2C5 recognizes an epitope on the outer surface of the RBD in a conformation which causes appreciable steric clashes with the RBD-bound ACE2, at least partly explaining the mechanism of neutralization. Interestingly, the P2C5 epitope is located on the other side of the RBD surface compared with the location of Leu455 and Phe456 residues, and therefore the activity of this antibody is not expected to be affected by the recently described, adjacent residue-flipping mutations L455F and F456L, which synergistically knock out many antibodies [6, 17].

Furthermore, the developed interface between P2C5 and RBD covering ~940 Å^2 area, as calculated using PISA [28], revealed many polar and hydrophobic contacts apparently stabilizing the interaction. For example, Arg357 and Glu471 of the RBD formed salt bridges with Glu104 and Arg52 of P2C5, respectively, Tyr449 of the RBD formed π–cation interaction with the side chain of Arg45 of P2C5, and also a range of intersubunit H-bonds were observed (Fig. 4a). Interestingly, the interface featured a hydrophobic core involving clustered aromatic residues from both RBD (e.g., Phe490, Tyr351) and P2C5 (e.g., Tyr37, Phe47, Trp111, Trp98) and also a few aliphatic hydrophobic residues among which Leu452 of RBD is the most prominent. Intriguingly, this residue is known to become mutated in the Delta variant (Fig. 4b) and therefore its location in the center of the interface with P2C5 nanobody suggested immediate consequences of the Leu452 mutation on the stability of the complex. Indeed, while the second Delta mutation, T478K, is located on the outer surface of RBD and cannot directly affect the interaction with P2C5, L452R is the mutation which presumably leads to the placement of the bulky, positively charged Arg side chain opposite to the long positively charged side chain of Lys96 of P2C5, unavoidably causing electrostatic repulsion and severe steric clashes especially given that the side chain of Lys96 is firmly sandwiched between the side chains of Trp98 and Trp111 of P2C5 (Fig. 4c). This obviously unfavorable configuration nicely explains the evasion of the Delta variant from the action of P2C5 nanobody.

We also noticed that two heavily mutated Omicron variants, B.1.1.529 and XBB.1 (Fig. 4b), among which only the former is efficiently recognized by P2C5 nanobody, share the E484A mutation located in the RBD:P2C5 interface (Fig. 4a). While Glu484 could be involved in making a polar contact with the side chain of Thr60 of P2C5, its substitution with Ala can break this polar contact and potentially destabilize the RBD:P2C5 binding. Nevertheless, this effect seems to be rather weak on its own, since this sole interfacial mutation in Omicron B.1.1.529 cannot prevent P2C5 from efficiently recognizing the corresponding RBD (Table 1). In this respect, P2C5 surpasses a recently described neutralizing nanobody 2S-1-19 in that the latter had lost the ability to recognize Omicron BA.1 (the same mutations as in B.1.1.529) [19]. Mutation of this Glu484 to lysine in Gamma RBD apparently is dispensable for the P2C5 binding as well, especially since the charge reversal at the 484 position in Gamma RBD (E484K) can make an additional, weak salt bridge with Glu46 of P2C5 (Fig. 4b). By exclusion, this indicates that the key role in destabilizing the RBD:P2C5 interaction in the case of Omicron XBB.1 RBD is played by the F490S mutation (Fig. 4, a-c). Indeed, as mentioned, Phe490 is located right in the hydrophobic cluster stabilizing the RBD:P2C5 interface and its side chain is stacked with the opposite Phe47 side chain of P2C5, whereas the removal of the aromatic Phe490 functionality would clearly compromise the cluster stability, especially accompanied by the introduction of the short polar side chain of a serine (Fig. 4c). Most delightfully, the role of other, numerous mutations found in the Omicron XBB.1 variant RBD can be neglected since all those are located beyond the region directly involved in the formation of the RBD:P2C5 interface, which fortunately excludes the necessity of conducting sophisticated combinatorial biochemical assays for assignment of the contribution of these mutations.

To sum up, our structural data explain the likely mechanism of the neutralization activity of the P2C5 nanobody on most of the earlier SARS-CoV-2 variants circulating before the emergence of Delta. Furthermore, the crystal structure obtained has allowed us to narrow the extended list of more recently emerged mutations, for example, found in the Delta and Omicron XBB.1 variants, potentially affecting the neutralization activity of P2C5, down to just two mutations, L452R and F490S, which rationalize the evasion of the Delta and Omicron XBB.1 variants of RBD from the action of P2C5. Interestingly, these mutations interfere with the RBD recognition by other nanobodies including the recently reported 2S-1-19 nanobody [19], despite the appreciably different footprints on RBD of this nanobody and P2C5 (Fig. 5). Last but not least, we expect that the crystal structure obtained can support P2C5 reengineering aimed at compensation for the effects of the new RBD mutations [7] and also can facilitate mapping of epitopes of other neutralizing antibodies against RBD in competition assays, even without requiring determination of new structures.

Contributions. N.N.S., D.V.S., and D.Y.L. initiated the project, I.A.F., I.V.D., A.I.K., I.A.A., I.B.E., A.A.D., V.V.P., and I.D.Z. obtained RBD variants and antibody, performed functional, *in vitro* and neutralization tests, N.N.S. prepared and purified complexes for

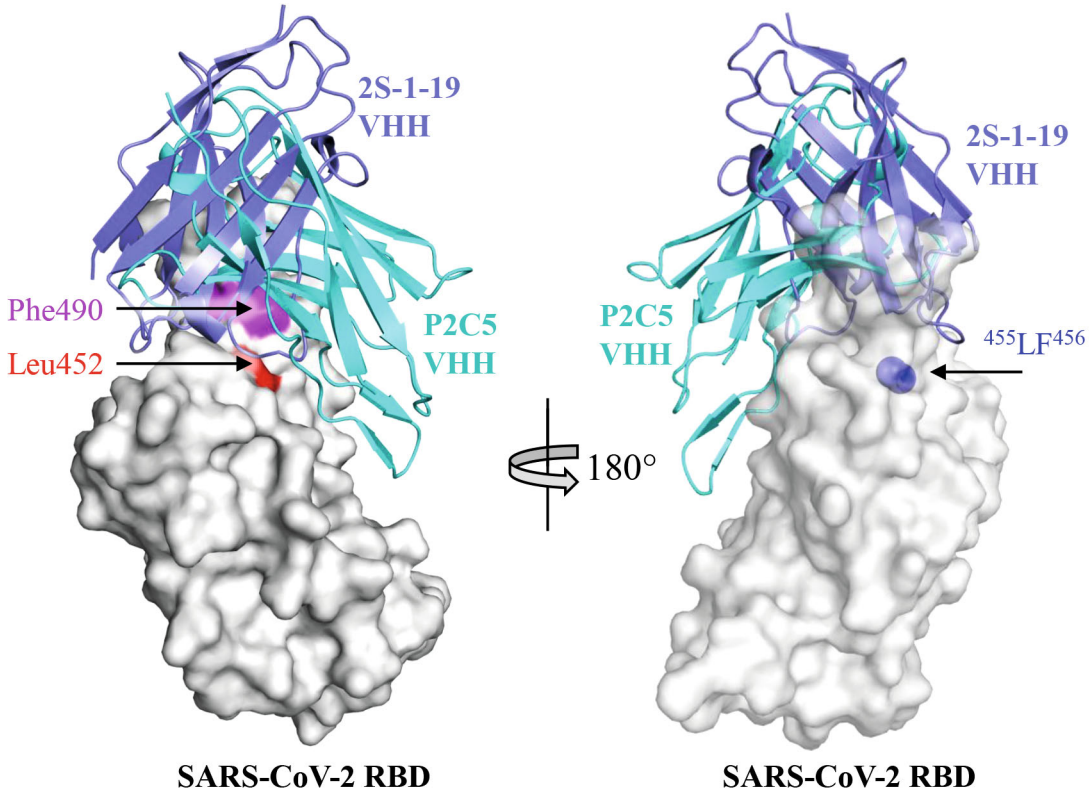

Fig. 5. Comparison of the RBD binding modes for nanobodies P2C5 (this work) and 2S-1-19 (PDB ID 8H91 [19]). The two crystal structures were superimposed by aligning RBD so that the different orientation and binding footprints are seen. The two projections are presented. Location of the residues Leu452 and Phe490 mutated in Delta and Omicron XBB variants are indicated. The residues Leu455-Phe456, mutated in newest SARS-CoV-2 variants to Phe455-Leu456 and thereby knocking out many antibodies [6], are shown by blue spheres representing their Cα atoms. Of note, P2C5 antibody binds from the other side of RBD and should not be sensitive to these mutations.

crystallization, L.A.V. crystallized protein complex, L.A.V. and K.M.B. collected X-ray data, N.N.S. solved structures, N.N.S. and L.A.V. refined structures, N.N.S., L.A.V., and K.M.B. validated structures, N.N.S. analyzed and compared structures, wrote the paper with input from all authors, D.V.S., D.Y.L., A.L.G., and V.O.P supervised the study, V.O.P. acquired funding.

Funding. The study was financially supported by the Russian Science Foundation (project no. 23-74-30004).

Ethics declarations. This work does not contain any studies involving human and animal subjects. The authors of this work declare that they have no conflicts of interest.

REFERENCES

1. Kansagra, K., Parmar, D., Mendiratta, S. K., Patel, J., Joshi, S., Sharma, N., Parihar, A., Bhoge, S., Patel, H., Kalita, P., Munshi, R., Kurmi, P., Shah, R., Gupta, A., Bhalla, H., Bekkalele, H., Verma, R., Agarwal, D., Sharma, S., Gawande, A., et al. (2021) A phase 3, randomized, open-label, noninferiority trial evaluating anti-rabies monoclonal antibody cocktail (TwinrabTM) Against Human Rabies Immunoglobulin (HRIG), *Clin. Infect. Dis.*, **73**, e2722-e2728, https://doi.org/10.1093/cid/ciaa779.
2. Hammitt, L. L., Dagan, R., Yuan, Y., Baca Cots, M., Bosheva, M., Madhi, Sh. A., Muller, W. J., Zar, H. J., Brooks, D., Grenham, A., Wählby, H. U., Mankad, V. S., Ren, P., Takas, T., Abram, M. E., Leach, A., Griffin,

M. P., and Villafana, T. (2022) Nirsevimab for prevention of RSV in healthy late-preterm and term infants, *New Eng. J. Med.*, **386**, 837-846, https://doi.org/10.1056/NEJMoa2110275.

3. Mulangu, S., Dodd Lori, E., Davey Richard, T., Tshiani Mbaya, O., Proschan, M., Mukadi, D., Lusakibanza, M. M., Nzolo, D., Tshomba, O. A., Ibanda, A., Ali, R., Coulibaly, S., Levine Adam, C., Grais, R., Diaz, J., Lane, H. C., and Muyembe-Tamfum, J.-J. (2019) A randomized, controlled trial of Ebola virus disease therapeutics, *New Eng. J. Med.*, **381**, 2293-2303, https://doi.org/10.1056/NEJMoa1910993.
4. Wang, Q., and Zhang, L. (2020) Broadly neutralizing antibodies and vaccine design against HIV-1 infection, *Front. Med.*, **14**, 30-42, https://doi.org/10.1007/s11684-019-0721-9.
5. Jarmo, O., Veli-Jukka, A., and Eero, M. (2020) Treatment of Clostridioides (Clostridium) difficile infection, *Ann. Med.*, **52**, 12-20, https://doi.org/10.1080/07853890.2019.1701703.
6. Liu, C., Das, R., Dijokaite-Guraliuc, A., Zhou, D., Mentzer, A. J., Supasa, P., Selvaraj, M., Duyvesteyn, H. M. E., Ritter, T. G., Temperton, N., Klenerman, P., Dunachie, S. J., Paterson, N. G., Williams, M. A., Hall, D. R., Fry, E. E., Mongkolsapaya, J., Ren, J., Stuart, D. I., and Screaton, G. R. (2024) Emerging variants develop total escape from potent monoclonal antibodies induced by BA.4/5 infection, *Nat. Commun.*, **15**, 3284, https://doi.org/10.1038/s41467-024-47393-3.
7. Laroche, A., Orsini Delgado, M. L., Chalopin, B., Cuniasse, P., Dubois, S., Sierocki, R., Gallais, F., Debroas, S., Bellanger, L., Simon, S., Maillère, B., and Nozach, H. (2022) Deep mutational engineering of broadly-neutralizing nanobodies accommodating SARS-CoV-1 and 2 antigenic drift, *mAbs*, **14**, 2076775, https://doi.org/10.1080/19420862.2022.2076775.
8. Hannula, L., Kuivanen, S., Lasham, J., Kant, R., Kareinen, L., Bogacheva, M., Strandin, T., Sironen, T., Hepojoki, J., Sharma, V., Saviranta, P., Kipar, A., Vapalahti, O., Huiskonen, J. T., and Rissanen, I. (2024) Nanobody engineering for SARS-CoV-2 neutralization and detection, *Microbiol. Spectrum*, **12**, e04199-04122, https://doi.org/10.1128/spectrum.04199-22.
9. Hanke, L., Vidakovics Perez, L., Sheward, D. J., Das, H., Schulte, T., Moliner-Morro, A., Corcoran, M., Achour, A., Karlsson Hedestam, G. B., Hällberg, B. M., Murrell, B., and McInerney, G. M. (2020) An alpaca nanobody neutralizes SARS-CoV-2 by blocking receptor interaction, *Nat. Commun.*, **11**, 4420, https://doi.org/10.1038/s41467-020-18174-5.
10. Hoffmann, M., Kleine-Weber, H., Schroeder, S., Krüger, N., Herrler, T., Erichsen, S., Schiergens, T. S., Herrler, G., Wu, N.-H., Nitsche, A., Müller, M. A., Drosten, C., and Pöhlmann, S. (2020) SARS-CoV-2 cell entry depends on ACE2 and TMPRSS2 and is blocked by a clinically proven protease inhibitor, *Cell*, **181**, 271-280.e278, https://doi.org/10.1016/j.cell.2020.02.052.
11. Lan, J., Ge, J., Yu, J., Shan, S., Zhou, H., Fan, S., Zhang, Q., Shi, X., Wang, Q., Zhang, L., and Wang, X. (2020) Structure of the SARS-CoV-2 spike receptor-binding domain bound to the ACE2 receptor, *Nature*, **581**, 215-220, https://doi.org/10.1038/s41586-020-2180-5.
12. Piccoli, L., Park, Y.-J., Tortorici, M. A., Czudnochowski, N., Walls, A. C., Beltramello, M., Silacci-Fregni, C., Pinto, D., Rosen, L. E., Bowen, J. E., Acton, O. J., Jaconi, S., Guarino, B., Minola, A., Zatta, F., Sprugasci, N., Bassi, J., Peter, A., De Marco, A., Nix, J. C., et al. (2020) Mapping neutralizing and immunodominant sites on the SARS-CoV-2 spike receptor-binding domain by structure-guided high-resolution serology, *Cell*, **183**, 1024-1042.e1021, https://doi.org/10.1016/j.cell.2020.09.037.
13. Xiang, Y., Nambulli, S., Xiao, Z., Liu, H., Sang, Z., Duprex, W. P., Schneidman-Duhovny, D., Zhang, C., and Shi, Y. (2020) Versatile and multivalent nanobodies efficiently neutralize SARS-CoV-2, *Science*, **370**, 1479-1484, https://doi.org/10.1126/science.abe4747.
14. Esmagambetov, I. B., Ryabova, E. I., Derkaev, A. A., Shcheblyakov, D. V., Dolzhikova, I. V., Favorskaya, I. A., Grousova, D. M., Dovgiy, M. A., Prokofiev, V. V., Gosudarev, A. I., Byrikhina, D. V., Zorkov, I. D., Iliukhina, A. A., Kovyrshina, A. V., Shelkov, A. Y., Naroditsky, B. S., Logunov, D. Y., and Gintsburg, A. L. (2023) rAAV expressing recombinant antibody for emergency prevention and long-term prophylaxis of COVID-19, *Front. Immunol.*, **14**, 1129245, https://doi.org/10.3389/fimmu.2023.1129245.
15. Favorskaya, I. A., Shcheblyakov, D. V., Esmagambetov, I. B., Dolzhikova, I. V., Alekseeva, I. A., Korobkova, A. I., Voronina, D. V., Ryabova, E. I., Derkaev, A. A., Kovyrshina, A. V., Iliukhina, A. A., Botikov, A. G., Voronina, O. L., Egorova, D. A., Zubkova, O. V., Ryzhova, N. N., Aksenova, E. I., Kunda, M. S., Logunov, D. Y., Naroditsky, B. S., et al. (2022) Single-domain antibodies efficiently neutralize SARS-CoV-2 variants of concern, *Front. Immunol.*, **13**, 822159, https://doi.org/10.3389/fimmu.2022.822159.
16. Deshpande, A., Harris, B. D., Martinez-Sobrido, L., Kobie, J. J., and Walter, M. R. (2021) Epitope classification and RBD binding properties of neutralizing antibodies against SARS-CoV-2 variants of concern, *Front. Immunol.*, **12**, 691715, https://doi.org/10.3389/fimmu.2021.691715.
17. Jian, F., Feng, L., Yang, S., Yu, Y., Wang, L., Song, W., Yisimayi, A., Chen, X., Xu, Y., Wang, P., Yu, L., Wang, J., Liu, L., Niu, X., Wang, J., Xiao, T., An, R., Wang, Y., Gu, Q., Shao, F., et al. (2023) Convergent evolution of SARS-CoV-2 XBB lineages on receptor-binding domain 455-456 synergistically enhances antibody evasion

and ACE2 binding, *PLOS Pathogens*, **19**, e1011868, https://doi.org/10.1371/journal.ppat.1011868.

18. Yang, J., Lin, S., Sun, H., Chen, Z., Yang, F., Lin, X., Guo, L., Wang, L., Wen, A., Zhang, X., Dai, Y., He, B., Cao, Y., Dong, H., Liu, X., Chen, B., Li, J., Zhao, Q., and Lu, G. (2022) A potent neutralizing nanobody targeting the spike receptor-binding domain of SARS-CoV-2 and the structural basis of its intimate binding, *Front. Immunol.*, **13**, 820336, https://doi.org/10.3389/fimmu.2022.820336.
19. Zhang, Y., Wang, D., Xiang, Q., Hu, X., Zhang, Y., Wu, L., Zhang, Z., Wang, Y., Zhao, J., McCormick, P. J., Fu, J., Fu, Y., Zhang, J., Jiang, H., and Li, J. (2024) A potent neutralizing nanobody targeting a unique epitope on the receptor-binding domain of SARS-CoV-2 spike protein, *Virology*, **589**, 109925, https://doi.org/10.1016/j.virol.2023.109925.
20. Boyko, K. M., Varfolomeeva, L. A., Egorkin, N. A., Minyaev, M. E., Alekseeva, I. A., Favorskaya, I. A., Ryabova, E. I., Prokofiev, V. V., Esmagambetov, I. B., Shcheblyakov, D. B., Logunov, D. Y., Gintsburg, A. L., Popov, V. O., and Sluchanko, N. N. (2023) Preparation and crystallographic analysis of a complex of SARS-CoV-2 S-protein receptor-binding domain with a virus-neutralizing nanoantibody, *Crystallogr. Rep.*, **68**, 864-871, https://doi.org/10.1134/S1063774523601168.
21. Vagin, A., and Teplyakov, A. (2010) Molecular replacement with MOLREP, *Acta Crystallogr. D Biol. Crystallogr.*, **66**, 22-25, https://doi.org/10.1107/S0907444909042589.
22. Jumper, J., Evans, R., Pritzel, A., Green, T., Figurnov, M., Ronneberger, O., Tunyasuvunakool, K., Bates, R., Zidek, A., Potapenko, A., Bridgland, A., Meyer, C., Kohl, S. A. A., Ballard, A. J., Cowie, A., Romera-Paredes, B., Nikolov, S., Jain, R., Adler, J., Back, T., et al. (2021) Highly accurate protein structure prediction with AlphaFold, *Nature*, **596**, 583-589, https://doi.org/10.1038/s41586-021-03819-2.
23. Murshudov, G. N., Skubák, P., Lebedev, A. A., Pannu, N. S., Steiner, R. A., Nicholls, R. A., Winn, M. D., Long, F., and Vagin, A. A. (2011) REFMAC5 for the refinement of macromolecular crystal structures, *Acta Cryst. D*, **67**, 355-367, https://doi.org/10.1107/S0907444911001314.
24. Emsley, P., and Cowtan, K. (2004) Coot: model-building tools for molecular graphics, *Acta Crystallogr. D Biol. Crystallogr.*, **60**, 2126-2132, https://doi.org/10.1107/S0907444904019158.
25. Shi, Z., Li, X., Wang, L., Sun, Z., Zhang, H., Chen, X., Cui, Q., Qiao, H., Lan, Z., Zhang, X., Li, X., Li, L., Xu, J., Gong, R., Fan, C., and Geng, Y. (2022) Structural basis of nanobodies neutralizing SARS-CoV-2 variants, *Structure*, **30**, 707-720.e705, https://doi.org/10.1016/j.str.2022.02.011.
26. Park, Y.-J., Pardon, E., Wu, M., Steyaert, J., and Hol, W. G. J. (2012) Crystal structure of a heterodimer of editosome interaction proteins in complex with two copies of a cross-reacting nanobody, *Nucleic Acids Res.*, **40**, 1828-1840, https://doi.org/10.1093/nar/gkr867.
27. Abramson, J., Adler, J., Dunger, J., Evans, R., Green, T., Pritzel, A., Ronneberger, O., Willmore, L., Ballard, A. J., Bambrick, J., Bodenstein, S. W., Evans, D. A., Hung, C.-C., O'Neill, M., Reiman, D., Tunyasuvunakool, K., Wu, Z., Žemgulytė, A., Arvaniti, E., Beattie, C., et al. (2024) Accurate structure prediction of biomolecular interactions with AlphaFold 3, *Nature*, **630**, 493-500, https://doi.org/10.1038/s41586-024-07487-w.
28. Krissinel, E., and Henrick, K. (2007) Inference of macromolecular assemblies from crystalline state, *J. Mol. Biol.*, **372**, 774-797, https://doi.org/10.1016/j.jmb.2007.05.022.